Ultrasound Shear Wave Viscoelastography: Model-Independent Quantification of the Complex Shear Modulus

Siavash Kazemirad, Simon Bernard, Samuel Hybois, An Tang, and Guy Cloutier, *Senior Member, IEEE*

***Abstract*— Ultrasound shear wave elastography methods are commonly used for estimation of mechanical properties of soft biological tissues in diagnostic medicine. A limitation of most currently used elastography methods is that they yield only the shear storage modulus (G') but not the loss modulus (G''). Therefore, no information on viscosity or loss tangent ($\tan\delta$) is provided. In this paper, an ultrasound shear wave viscoelastography method is developed for model-independent quantification of frequency-dependent viscoelastic complex shear modulus of macroscopically homogeneous tissues. Three *in vitro* tissue-mimicking phantoms and two *ex vivo* porcine liver samples were evaluated. Shear waves were remotely induced within the samples using several acoustic radiation force pushes to generate a semicylindrical wave field similar to those generated by most clinically used elastography systems. The complex shear modulus was estimated over a broad frequency range (up to 1000 Hz) through the analytical solution of the developed inverse wave propagation problem using the measured shear wave speed and amplitude decay versus propagation distance. The shear storage and loss moduli obtained for the *in vitro* phantoms were compared with those from a planar shear wave method and the average differences over the whole frequency range studied were smaller than 7% and 15%, respectively. The reliability of the proposed method highlights its potential for viscoelastic tissue characterization, which may improve noninvasive diagnosis.**

***Index Terms*— Dynamic elastography, elasticity and viscosity, inverse problem solution, ultrasound imaging, viscoelastic properties, viscoelasticity.**

Manuscript received April 14, 2016; accepted June 17, 2016. Date of publication June 28, 2016; date of current version September 12, 2016. This work was supported in part by the Institute of Nutrition, Metabolism and Diabetes of the Canadian Institutes of Health Research under Grant 273738 and Grant 301520, and in part by the Fonds de Recherche du Québec–Nature et Technologies under Grant PR-174387. *(Corresponding author: Guy Cloutier.)*

S. Kazemirad, S. Bernard, and S. Hybois are with the Laboratory of Biorheology and Medical Ultrasonics, Montreal, QC H2X 0A9, Canada, and also with the University of Montreal Hospital Research Center, Montreal, QC H2X 0A9, Canada (e-mail: siavash.kazemirad@mail.mcgill.ca; s.bernard.simon@gmail.com; samuel.hybois@mines-nancy.org).

A. Tang is with the University of Montreal Hospital Research Center, Montreal, QC H2X 0A9, Canada, also with the Department of Radiology, University of Montreal Hospital, Montreal, QC H2X 0A9, Canada, and also with the Department of Radiology, Radio-Oncology and Nuclear Medicine, Université de Montréal, Montreal, QC H3T 1J4, Canada (e-mail: duotango@videotron.ca).

G. Cloutier is with the Laboratory of Biorheology and Medical Ultrasonics, Montreal, QC H2X 0A9, Canada, also with the University of Montreal Hospital Research Center, Montreal, QC H2X 0A9, Canada, also with the Department of Radiology, Radio-Oncology and Nuclear Medicine, Université de Montréal, Montreal, QC H3T 1J4, Canada, and also with the Institute of Biomedical Engineering, Université de Montréal, Montreal, QC H3T 1J4, Canada (e-mail: guy.cloutier@umontreal.ca).

Digital Object Identifier 10.1109/TUFFC.2016.2583785

I. Introduction

SHEAR wave elastography methods are developed to assess mechanical properties of soft tissues [1], [2]. Shear waves are generated by acoustic radiation force in ultrasound-based dynamic elastography clinical systems [3], [4]. Most commonly, several shear wave fields are generated by rapidly moving the location of the focused radiation force push axially [5], [6]. The interaction of these shear wave fields generates a semicylindrical wavefront with a propagation direction perpendicular to the pushing axis. When the speed of generated focused pushes is significantly higher than that of propagating shear waves (e.g., with the Mach number typically higher than 10), the global (superposed) shear wave field tends to an ideal cylindrical shape with parallel fronts observed in 2-D ultrasound images [4].

The tissue mechanical properties provide information about their pathological condition and have been clinically used for diagnostic purposes in numerous organs such as liver, breast, thyroid, bowel, pancreas, prostate, lymph nodes, and tendons [7]–[11]. A limitation of most current elastography methods is that only shear wave speed is measured, and thus only the storage modulus (G') can be directly estimated from the inverse problem solution. However, other properties such as loss modulus (G''), from which viscosity can be estimated, may be required for tissue characterization [12]–[14]. Using magnetic resonance elastography (MRE), Garteiser *et al.* [12] assessed the viscoelastic properties of human liver tumors and found that the loss modulus provided a better discrimination between benign and malignant tumors than the storage modulus. Streitberger *et al.* [14] estimated the viscoelasticity of human brain parenchyma for presurgical assessment in glioblastoma using MRE and obtained lower viscosities for glioblastomas than normal tissues. Therefore, viscosity (and thus loss modulus) may help in the classification of brain tumors as well. Although ultrasound elastography measurement of the brain may be difficult to perform, recent studies have shown promise for this specific application of elastography [15], [16]. For example, Chauvet *et al.* [16] reported the elasticity of normal brain parenchyma and brain tumors obtained intraoperatively by shear wave elastography in 63 patients and concluded that intraoperative ultrasound elastography of brain tumors may improve diagnosis and guide the resection.

Approximate rheological models may be fitted to measured shear wave speeds to obtain the complex shear modulus (i.e., storage and loss moduli) [17]–[20]. Oestreicher [17] developed equations for wave propagation in a viscoelastic medium considering a Voigt model. Chen *et al.* [19] proposed a method to estimate the complex shear modulus of viscoelastic materials through cylindrical shear wave dispersion ultrasound vibrometry, also using the Voigt model. Other rheological models such as Maxwell, Jeffrey, and Zener were also used in the prior literature to investigate which model better fits to the experimental data [21]. Yet, these models may not accurately describe the behavior of different types of normal and pathological soft tissues. Hence, the development of a noninvasive model-independent characterization method remains of great interest.

Only a few model-independent viscoelasticity measurement methods have been proposed to date, each with limitations that may have hindered their clinical adoption [22]–[27]. Catheline *et al.* [22] proposed a method to estimate viscoelastic properties of soft materials using an inverse problem algorithm for the case of planar shear waves generated by a plate connected to an external vibrator. Vappou *et al.* [23] developed an approach based on harmonic motion imaging to measure both storage and loss moduli using the phase shift between shear stress and strain. They made an assumption of harmonic plane shear wave propagation and obtained viscoelastic properties over a limited frequency range. More recently, Amador *et al.* [24] proposed a local quantification of the complex shear modulus of viscoelastic materials through the measurement of acoustic radiation force induced creep. The measurements needed to be performed at several different locations to obtain the global viscoelastic properties of the tissue or a viscoelasticity map if desired. Kazemirad *et al.* [25] proposed a method for model-independent characterization of viscoelastic properties of soft materials using the surface Rayleigh wave propagation, which can only be used for *in vitro* or superficial *in vivo* measurements. Nenadic *et al.* [27] presented a method based on 2-D fast Fourier transform (2-D FFT) to obtain frequency-dependent shear wave speed and attenuation for planar and cylindrical shear wave propagations in viscoelastic materials. It was shown that the 2-D FFT analysis may yield biased results for the shear wave speed and attenuation, although the biases can be reduced considering the aspect ratio of the excitation and material properties [28]. Furthermore, the application of this method, which works based on the full-width-at-half maximum of 2-D FFT graph along the k-axis, may be limited in the case of *in vivo* measurements with noisy 2-D FFT graphs, such as the one obtained for *in vivo* measurements of a porcine bladder [29].

In some studies, the inverse problem of shear wave scattering from a mechanical inclusion has been analytically solved to obtain the viscoelastic properties of the propagation media [30]–[32]. For example, Montagnon *et al.* [32] presented a method to assess the viscoelastic properties of a spherical scatterer embedded in a macroscopically homogeneous medium. These analytical methods, however, depend on a set of *a priori* assumptions such as the exact location and geometry of the inclusion.

The purpose of this paper was to develop an ultrasound shear wave viscoelastography method for model-independent quantification of the frequency-dependent complex shear modulus of soft tissues and biomaterials. The proposed method assumes a macroscopically homogeneous and isotropic propagation medium and a cylindrical shear wave field as generated by most clinically used elastography systems. Three *in vitro* tissue mimicking phantoms and two *ex vivo* porcine liver samples were tested. An implementation of the beam sequence similar to the supersonic shear imagine (SSI) technology was used for shear wave generation [4]. An analytical complex model was developed for the inverse wave propagation problem of the generated semicylindrical shear wave fields, considering both shear wave speed and amplitude decay versus propagation distance. The complex inverse problem was then solved numerically in the frequency domain using an optimization method to obtain the real and imaginary parts of the shear wavenumber at each frequency, resulting in the estimation of storage and loss moduli over a broad range of frequencies (up to 1000 Hz). The results were compared with the shear storage moduli obtained by conventional shear wave elastography and with the shear storage and loss moduli assuming a planar shear wave propagation obtained using a plate connected to an external vibrator.

II. Methods and Materials

A. Inverse Wave Propagation Problem

In the absence of body forces, Navier's equation governing the wave motion in isotropic, linear, and macroscopically homogeneous viscoelastic media is given as [33]

$$\rho \frac{\partial^2 \mathbf{u}}{\partial t^2} = \hat{\mu} \nabla^2 \mathbf{u} + (\hat{\lambda} + \hat{\mu}) \nabla (\nabla \cdot \mathbf{u}) \tag{1}$$

where ρ is the mass density of the propagation medium, $\mathbf{u}$ is the displacement vector, and $\hat{\lambda}$ and $\hat{\mu}$ are complex and frequency-dependent viscoelastic Lamé coefficients. Under the assumption of pure shear wave propagation, where the direction of particle displacements is perpendicular to the wave propagation direction, the divergence of the displacement vector vanishes so that $\nabla \cdot \mathbf{u} = 0$. Navier's equation (1) is hence simplified to

$$\rho \frac{\partial^2 \mathbf{u}}{\partial t^2} = \hat{\mu} \nabla^2 \mathbf{u}. \tag{2}$$

In the case of cylindrical shear wave propagation, where $u_z \neq 0$ and $u_r = u_\theta = 0$ (Fig. 1), the solution of (2) in the frequency domain is given as [34]

$$\hat{U}_z(r, \omega) = a(\omega) \frac{i}{4} H_0^1(\hat{k}_s(\omega) r) \tag{3}$$

where ω is the angular frequency, $a(\omega)$ is related to the amplitude of shear waves at different frequencies, $H_0^1(X)$ is the Hankel function of the first kind of order zero, r is the propagation distance in the radial direction of the assumed cylindrical coordinate system, and $\hat{k}_s(\omega)$ is the complex frequency-dependent shear wavenumber, which may be

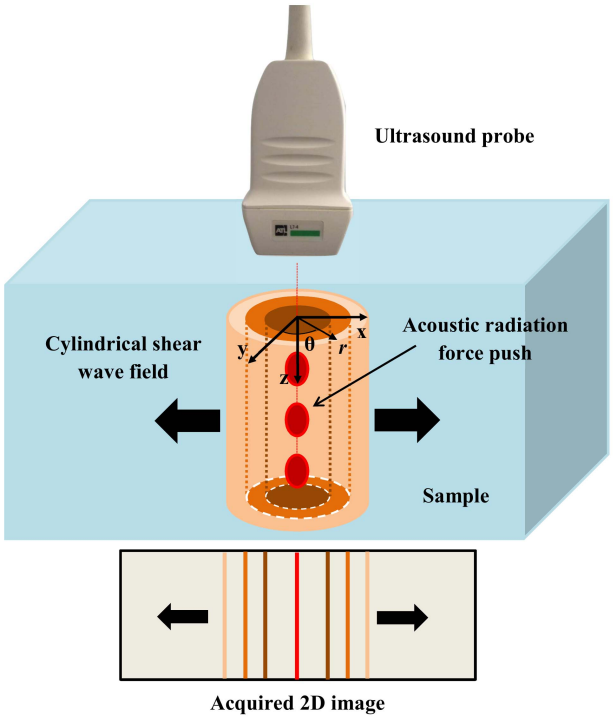

Fig. 1. Schematic of semicylindrical shear wave generation within the sample using acoustic radiation force pushes.

considered as $\hat{k}_s(\omega) = \alpha(\omega) - i\beta(\omega)$, where $\alpha(\omega) \geq 0$ and $\beta(\omega) \geq 0$. The total displacement at radius r in the time domain may be calculated using the inverse Fourier transform of the displacement in the frequency domain as

$$u_z(r,t) = \int \hat{U}_z(r,\omega) e^{i\omega t} d\omega. \tag{4}$$

Far enough from the z-axis of the assumed cylindrical shear wave field (i.e., from the origin of the wave field), where $\|\hat{k}_s(\omega)r\| \gg 0$, the asymptotic form of Hankel function is considered as [35]

$$H_0^1(\hat{k}_s(\omega)r) \approx \sqrt{\frac{2}{\pi \hat{k}_s(\omega)r}} e^{(-i(\hat{k}_s(\omega)r + \frac{\pi}{4}))}. \tag{5}$$

Substituting (5) into (3), and after some manipulations, the displacement in the frequency domain is obtained in terms of real and imaginary parts of the shear wavenumber as

$$\hat{U}_z(r,\omega) = \sqrt{\frac{a(\omega)^2}{8\pi r\sqrt{\alpha(\omega)^2+\beta(\omega)^2}}} \times e^{\left(-\beta(\omega)r - i\alpha(\omega)r + i\frac{\pi}{4} + i\tan^{-1}\sqrt{\frac{-\alpha(\omega)+\sqrt{\alpha(\omega)^2+\beta(\omega)^2}}{\alpha(\omega)+\sqrt{\alpha(\omega)^2+\beta(\omega)^2}}}\right)} \tag{6}$$

which may be rewritten as

$$\hat{U}_z(r,\omega) = A(\omega)\frac{e^{-\beta(\omega)r}}{\sqrt{r}} e^{-i(\alpha(\omega)r - \varphi_0)} \tag{7}$$

considering the frequency-dependent location-independent part of the displacement amplitude $A(\omega)$ and the initial phase angle at the origin φ_0 as

$$A(\omega) = \sqrt{\frac{a(\omega)^2}{8\pi\sqrt{\alpha(\omega)^2+\beta(\omega)^2}}} \tag{8a}$$

$$\varphi_0 = \frac{\pi}{4} + \tan^{-1}\sqrt{\frac{-\alpha(\omega)+\sqrt{\alpha(\omega)^2+\beta(\omega)^2}}{\alpha(\omega)+\sqrt{\alpha(\omega)^2+\beta(\omega)^2}}}. \tag{8b}$$

The displacement in the frequency domain may also be written in terms of the displacement amplitude $\|\hat{U}_z(r,\omega)\|$ and phase angle $\theta(\hat{U}_z(r,\omega))$ as

$$\hat{U}_z(r,\omega) = \|\hat{U}_z(r,\omega)\| e^{-i\theta(\hat{U}_z(r,\omega))}. \tag{9}$$

The displacement amplitude and phase angle can be experimentally obtained at different frequencies over a range of propagation distance. Then, the real and imaginary parts of the shear wavenumber at each frequency could be estimated through the numerical solution (least-squares fitting) of the following equations that are obtained from (7) and (9):

$$\mathrm{Ln}(\|\hat{U}_z(r,\omega)\|) = \mathrm{Ln}(\|A(\omega)\|) - \beta(\omega)r - \frac{\mathrm{Ln}(r)}{2} \tag{10a}$$

$$\theta(\hat{U}_z(r,\omega)) = \alpha(\omega)r - \varphi_0. \tag{10b}$$

For a linear and isotropic viscoelastic medium, the complex shear modulus $\hat{G}(\omega) = G'(\omega) + iG''(\omega)$ is related to the complex shear wavenumber through $\hat{G}(\omega) = \rho\omega^2/\hat{k}_s^2$. Therefore, the shear storage and loss moduli and the loss factor ($\tan\delta$) could be obtained using the estimated real and imaginary parts of the shear wavenumber as [23], [36]

$$G'(\omega) = \rho\omega^2 \frac{\alpha(\omega)^2 - \beta(\omega)^2}{[\alpha(\omega)^2+\beta(\omega)^2]^2} \tag{11a}$$

$$G''(\omega) = 2\rho\omega^2 \frac{\alpha(\omega)\beta(\omega)}{[\alpha(\omega)^2+\beta(\omega)^2]^2} \tag{11b}$$

$$\tan\delta(\omega) = \frac{G''(\omega)}{G'(\omega)} = \frac{2\alpha(\omega)\beta(\omega)}{\alpha(\omega)^2 - \beta(\omega)^2}. \tag{11c}$$

Under the same assumption of linear viscoelasticity, the dynamic viscosity (η) of the propagation medium is simply estimated by [36]

$$\eta(\omega) = \frac{G''(\omega)}{\omega}. \tag{12}$$

In conventional shear wave elastography, only the shear storage modulus (also called shear modulus or shear stiffness [37]) is estimated using the measured shear wave velocity ($c_s(\omega)$) through

$$G'_e(\omega) = \rho c_s^2(\omega) \tag{13}$$

where the shear wave velocity ($c_s(\omega)$) at different frequencies can be estimated in the wave number frequency domain (k-space) obtained using a 2-D Fourier transform of the time-domain displacement field with respect to temporal and spatial coordinates [38].

TABLE I
PERCENTAGE OF MATERIALS USED FOR THE FABRICATION OF *IN VITRO* PHANTOMS. PERCENTAGES ARE IN PROPORTION TO THE TOTAL MIXTURE WEIGHT

Phantoms	Gelatin	Agar	Castor oil	Glucosamine
Phantom #1	4	5	0	0
Phantom #2	4	5	10	0.2
Phantom #3	4	5	20	0.2

B. Sample Preparation

Three *in vitro* tissue-mimicking phantoms and two *ex vivo* porcine liver samples were tested by the proposed viscoelastography method. The *in vitro* phantoms were also tested with a planar shear wave propagation method, and viscoelastic properties were compared for evaluation purposes. The *ex vivo* liver sample measurements were performed shortly postmortem as a feasibility study to assess the ability of the proposed methodology to estimate the viscoelastic properties of physiological tissues.

The *in vitro* phantoms were fabricated with gelatin (G2500, Sigma–Aldrich chemical, St. Louis, MO, USA), agar (A9799, Sigma–Aldrich chemical), castor oil (259853, Sigma–Aldrich chemical), glucosamine (G8641, Sigma–Aldrich chemical), and water. Agar powder provided ultrasound wave scattering and castor oil was used to increase the viscosity (and thus the loss modulus) of the phantoms. Glucosamine was used to stabilize the emulsion and avoid the separation of water and castor oil [39]. The concentration of castor oil was varied for different phantoms to obtain a range of viscosity and, hence, of loss moduli. Table I summarizes material weight concentrations used for the fabrication of each phantom. Water was first heated to 90 °C, at which gelatin was gradually dissolved in water while smoothly stirring the mixture. When a transparent mixture with no floating gelatin particles was obtained, castor oil and glucosamine were added. Then, the mixture was gradually cooled down to 50 °C while stirring and agar powder was added. The medium was then further cooled down to room temperature. Air bubbles were removed from the gel using a vacuum chamber right before casting. Two liters of gel were prepared for each *in vitro* phantom, which was casted into a mold with approximate dimensions of $20 \times 10 \times 10$ cm^3 for both cylindrical and planar shear wave measurements. A plate used for planar shear wave experiments was placed within the mixture prior to gelation. The samples were kept in the refrigerator at a temperature of 4 °C for 18 h to ensure uniform gelation. Samples were subsequently kept at room temperature (22 °C) and under water for 6 h prior to measurements to avoid dehydration and to obtain a uniform temperature for all the samples.

C. Ultrasound Measurements

For both conventional ultrasound shear wave elastography and the proposed viscoelastography measurements, an implementation of a beam sequence similar to the SSI was used to generate shear waves within the samples [4]. A linear array transducer (ATL L7-4, Philips, Bothell, WA, USA) controlled by a research ultrasound system (Verasonics V1, Verasonics Inc., Redmond, WA, USA) was used to remotely generate the shear waves by acoustic radiation force. Each sequence was made of three focused pushes within the sample spaced 5 mm apart. The duration of each individual focused push was 100 μs, with a delay of 125 μs between the generations of consecutive pushes, resulting in a pushing velocity of 40 m/s. The corresponding Mach number (the ratio of pushing velocity to shear wave propagation velocity) was between 10 and 15, depending on the mechanical properties of different samples and hence the shear wave velocity. The ultrasound transducer excitation voltage was fixed at 30 V and the push duration was maintained at 100 μs for all the measurements. The same transducer was used to track the shear waves immediately after their generation using a fast plane wave imaging technique, which allowed a high frame rate acquisition of the radio-frequency data up to 4 kHz, as performed earlier [40]. Ten consecutive pushing and tracking sequences were performed for each tested sample. Three sequences with highest signal-to-noise ratios (SNRs) and thus less noisy displacement fields were chosen for postprocessing and results were averaged.

Shear wave displacement fields, needed for the inverse problem solution, were estimated from the acquired radio-frequency data using a 1-D normalized cross-correlation algorithm implemented on a graphic processing unit [41]. Three reference images were acquired before the pushing phase and used as reference images for the estimation of displacement fields. In the case of viscoelastography measurements with the proposed method, the shear storage and loss moduli were estimated from the proposed methodology using the measured amplitude and phase angle of displacement fields (10), (11). For conventional elastography measurements, however, only the shear storage modulus was estimated using the phase velocities obtained via the phase angles at different locations along the propagation distance (13).

The SNR was computed at each pixel using the displacement amplitude measured during shear wave propagation, $\|u_{zs}\|$, and the noise amplitude measured when no shear wave propagated, $\|u_{zn}\|$, through

$$\mathrm{SNR}_{dB} = 20\log_{10}\left(\frac{\|u_{zs}\|}{\|u_{zn}\|}\right). \tag{14}$$

A propagation distance of a few millimeters (about one wavelength) is normally needed for the shear waves generated by acoustic radiation force to be fully developed. Therefore, the postprocessing regions of interest (ROIs) were chosen from the location of the peak displacement amplitude to the pixel where the displacement amplitude tended to the background noise, determined based on a marginal SNR of 10 dB. The length of the ROIs was around 12 and 7 mm for *in vitro* and *ex vivo* samples, respectively, depending on the dissipation of the propagation media.

D. Validation

The planar shear wave experiments used for evaluation purposes were performed using an experimental setup similar

to that of [21]. The planar shear wave method was compared with conventional rheometry for *in vitro* hydrogel phantoms in [42], and the results were found in good agreement with an average correlation coefficient of 0.84 for the shear wave speed and 0.95 for the attenuation coefficient. One can thus conclude that good agreement exists for both storage and loss moduli. This indicates that the results obtained by this method may be considered as a benchmark for viscoelastic characterization of soft materials. An 8 cm × 10 cm Plexiglas plate was used for shear wave generation. This plate, which was chosen to be large enough to generate semiplanar shear waves at the frequencies of interest, was driven by a shaker (type 4810, Brüel & Kjær, Nærum, Denmark), which was itself connected to an arbitrary waveform generator (33250A, Agilent Technologies, Santa Clara, CA, USA) and a power amplifier (type 2706, Brüel & Kjær). Excitation signals were a 15 Vpp (peak-to-peak voltage), eight periods Blackman-windowed sinusoids at a central frequency starting at 200 Hz with 100 Hz increments. The maximum excitation frequency for which the results were exploitable varied depending on the phantom dissipation.

Tissue displacements were tracked using the plane wave imaging technique with a frame rate of 4 kHz for 60 ms immediately after the excitation of the plate. The 1-D cross-correlation algorithm was also used to quantify the displacements. A rectangular window was applied in the time domain, which allowed keeping the forward-propagating wave only. As the *in vitro* phantoms were relatively large and the generated waves were transient, such a window enabled discarding wave reflections from the phantom boundaries. The displacement signals were then converted to the frequency domain using the Fourier transform, and the phase and amplitude of the wave were extracted at the central frequency of the excitation signal. For a plane wave, the phase and the natural logarithm of the amplitude are linear functions of the propagation distance and a linear least-squares fit of these quantities yielded the shear wave velocity $c_s(\omega)$ and attenuation $\beta(\omega)$, respectively [21]. The complex shear wavenumber was then computed as $\hat{k}_s(\omega) = (\omega/c_s(\omega)) - i\beta(\omega)$, and the shear storage and loss moduli were obtained from (11). The experimental errors in the estimation of velocity and attenuation and, thus, shear and loss moduli were assessed via the standard deviation of the results of linear fits. This analysis was repeated for each excitation frequency of the plate.

To ensure the comparability of planar and cylindrical shear wave viscoelastography measurements, both experiments were performed at a close temporal window and for the exact same position of the ultrasound probe on the samples. Moreover, the postprocessing of the experimental data was performed at a 25-mm depth for both of the measurements, which was the center of the generated shear wavefronts in the case of *in vitro* phantoms. At this depth, the results were averaged over ten consecutive lines of each around 0.037 mm thick.

III. Results

Typical displacement maps generated in Phantom #1 and Liver #1 by the implemented ultrasound pushing sequence are shown in Fig. 2. The semiparallel shear wavefronts, induced

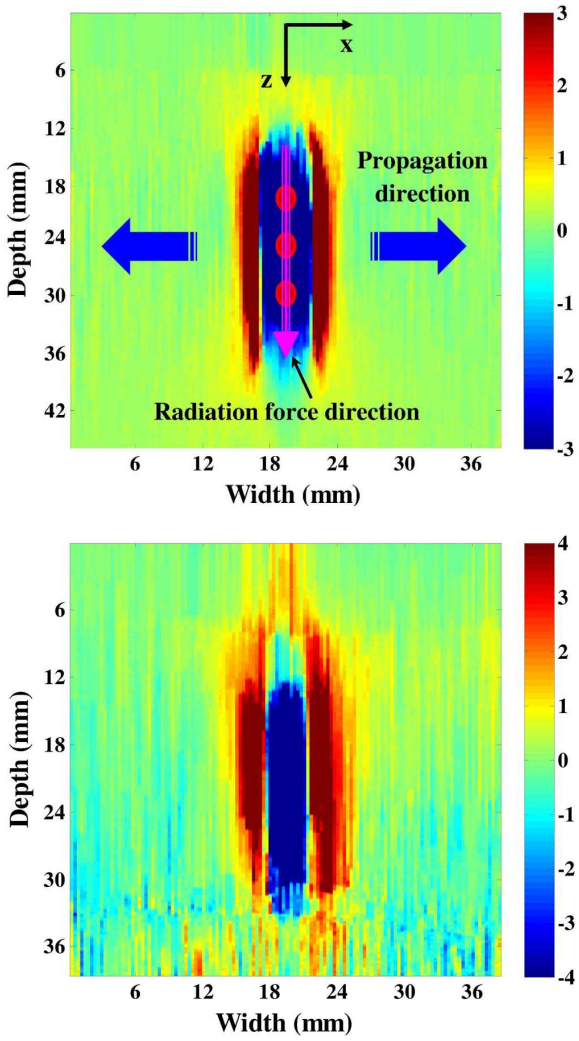

Fig. 2. Typical displacement maps in the z-direction (u_z) generated in Phantom #1 (top) and Liver #1 (bottom) using three acoustic radiation force pushes at 20-, 25-, and 30-mm depths for Phantom #1 and at 15-, 20-, and 25-mm depths for Liver #1. The displacement maps are shown at 1 and 2 ms after the generation of the last push in Phantom #1 and Liver #1, respectively. The displacement amplitude of the colorbars is given in micrometers.

by three focused pushes at depths of 20, 25, and 30 mm for Phantom #1 and at depths 15, 20, and 25 mm for Liver #1, indicate the propagation of a semicylindrical shear wave field in three dimensions. The maximum displacement amplitude and the SNR for these cases were about 3 μm and 20 dB, respectively. Fig. 3(a)–(c) shows the displacement amplitude generated in Phantom #1 at frequencies of 200, 400, and 600 Hz, respectively. As seen, the displacement amplitude was smaller at higher frequencies, where the wave amplitude decayed faster with propagation distance.

The shear storage and loss moduli for *in vitro* phantoms (Phantoms #1–#3) are shown in Fig. 4 over a frequency range from 200 to 1000 Hz. Except for Phantom #3, the planar shear wave method provided reliable results over the whole bandwidth. Overall, the results obtained with the proposed viscoelastography method were in good agreement with those of the reference methods (planar shear wave method and conventional elastography for G'). In the case of Phantom #1, differences between storage moduli of the proposed method

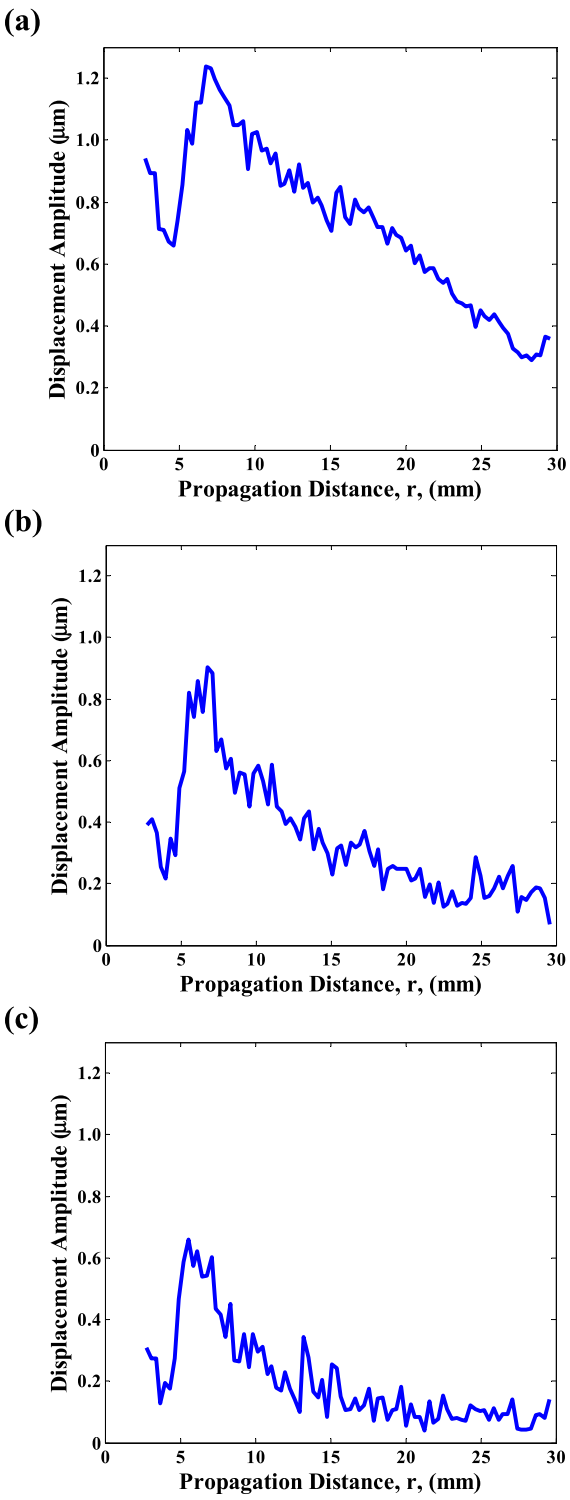

Fig. 3. Displacement amplitude in Phantom #1 along the propagation distance measured at single frequencies by computing the absolute value of the corresponding Fourier transform component. (a) 200 Hz. (b) 400 Hz. (c) 600 Hz.

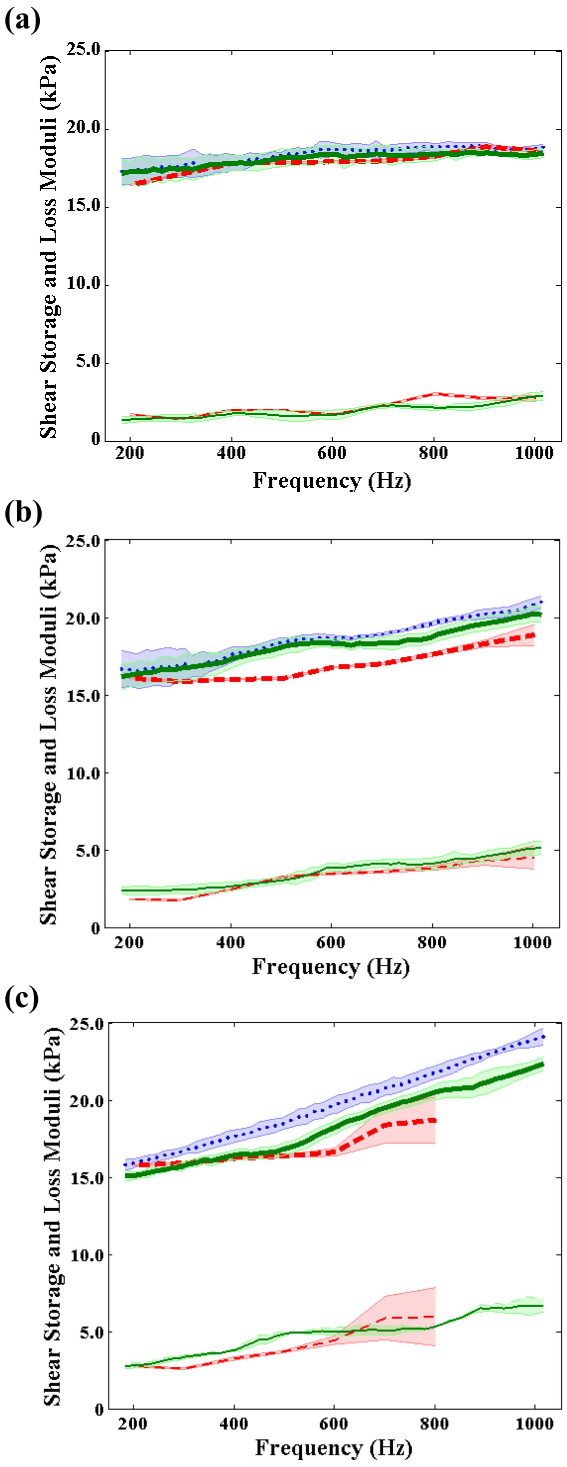

Fig. 4. Shear storage (G') and loss (G'') moduli estimated for (a) Phantom #1, (b) Phantom #2, and (c) Phantom #3 over a frequency range from 200 to 1000 Hz. ▬: G' for the proposed viscoelastography method. ▬ ▬: G' for the planar shear wave method. • • • • • • : G' for the conventional elastography. ▬: G'' for the proposed viscoelastography method. ▬ ▬ ▬ ▬: G'' for the planar shear wave method.

and benchmark measures were smaller than 3% (for conventional elastography) or 5% (for the planar shear wave method), respectively [Fig. 4(a)]. Differences in loss moduli between cylindrical and planar shear wave methods were smaller than 28%, with an average of 11% over the whole frequency range studied here. For Phantom #2, differences were smaller than 5% or 12% (average of 7%) between the storage moduli of the proposed method and elastography or planar shear wave measures, respectively, and smaller than 32% (average of 15%) for loss modulus comparisons with planar shear wave measurements [Fig. 4(b)]. The corresponding differences were

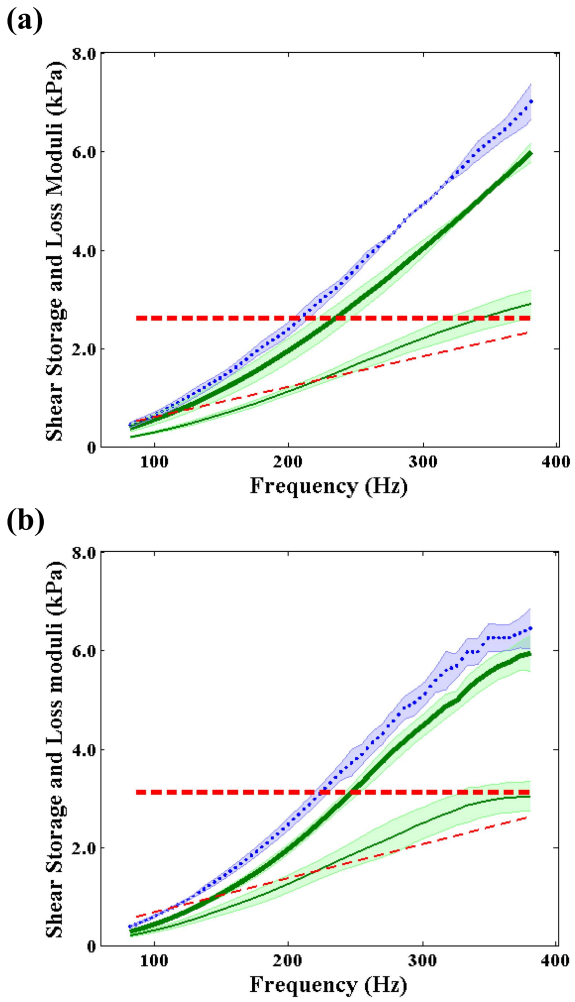

Fig. 5. Shear storage (G') and loss (G'') moduli estimated for (a) Liver #1 and (b) Liver #2 over a frequency range from 80 to 380 Hz. ▬: G' for the proposed viscoelastography method. ▬ ▬: G' for the Voigt fit. • • • • • • : G' for the conventional elastography. ▬: G'' for the proposed viscoelastography method. ▬ ▬ ▬ ▬: G'' for the Voigt fit.

smaller than 10% (average of 7%) or 10% (average of 5%), respectively, for storage moduli, and 26% (average of 15%) for loss moduli in the case of Phantom #3 [Fig. 4(c)]. The average tan δ values obtained using the proposed viscoelastography method over the whole frequency range for Phantom #1 (0% castor oil), Phantom #2 (10% castor oil), and Phantom #3 (20% castor oil) were 0.11 ± 0.02, 0.20 ± 0.04, and 0.26 ± 0.04 (mean $\pm$ standard deviation), respectively. This increase in tan δ with percentages of castor oil was accompanied by a greater slope of the shear storage modulus curve versus frequency, which was 1.49, 4.51, and 9.23 Pa/Hz for Phantoms #1–#3, respectively.

The shear storage and loss moduli for the two *ex vivo* liver samples (Livers #1 and #2) are shown in Fig. 5 over a frequency bandwidth of 80–380 Hz. The differences between storage moduli of the proposed method and elastography measures were smaller than 16% and 14% for Livers #1 and #2, respectively. The corresponding average tan δ values were 0.55 ± 0.03 and 0.62 ± 0.07, and the slopes of the shear storage modulus versus frequency were 17.5 and 21.0 Pa/Hz, respectively.

The average coefficients of variation (i.e., the ratio of the standard deviation to the mean value) for the shear storage moduli obtained with the proposed method were 2.8%, 2.8%, and 2.1% for Phantoms #1–#3, and 11.0% and 5.2% for Livers #1 and #2, respectively. The corresponding values for the shear loss moduli were 7.7%, 8.6%, 4.0%, 7.9%, and 13.2%, respectively.

The Voigt rheological model is commonly used in the literature to fit the viscoelastic properties of biological tissues [10], [19]. As a case study of the accuracy of such model, shear wave velocities within Livers #1 and #2 were fitted to the Voigt model and the shear elasticity and viscosity were estimated at 2.62 kPa and 0.98 Pa · s and 3.12 kPa and 1.10 Pa · s for the two *ex vivo* liver samples, respectively. Differences between the corresponding shear storage and loss moduli and those of the proposed model-independent viscoelastography method were, respectively, smaller than 564% (average of 107%) and 139% (average of 32%) for Liver #1 and 952% (average of 209%) and 161% (average of 58%) for Liver #2. These results are discussed in the following.

IV. Discussion

As shown in the prior MRE literature [12], [43] and also confirmed by the high tan δ values obtained for *ex vivo* liver samples in this paper, soft biological tissues can be highly viscoelastic, which emphasizes the importance of model-independent viscoelasticity assessment for diagnostic purposes. Besides, the case study of fitting the Voigt model to measured shear wave speeds to obtain the storage and loss moduli of *ex vivo* liver samples suggests that such approximate rheological modeling may not accurately describe the viscoelastic behavior of soft tissues.

The storage and loss moduli were obtained over a broad frequency range using the proposed shear wave viscoelastography method and were in good agreement with those of reference methods. The frequency ranges in which reliable results were obtained for *in vitro* and *ex vivo* samples were chosen based on the shear wave amplitude and SNR at different frequencies. In the case of *ex vivo* liver samples, generated shear waves, especially the high-frequency components, were dissipated more rapidly with distance than in *in vitro* phantoms. Therefore, the frequency range was narrower for these *ex vivo* samples.

Differences between the results obtained with the proposed method and the planar shear wave technique are likely related to experimental variability and noise and assumptions on cylindrical or planar wave propagation. Differences between the proposed method and conventional elastography, for G' estimation, may be explained by the assumption of zero dissipation in standard elastography. This assumption, which leads to a zero value for the imaginary part of the wavenumber (β) and consequently an overestimation of the shear storage modulus, is not a valid assumption for most biomaterials and soft tissues. This is explicitly observed by the comparison of (11a) and (13), where $c_s^2(\omega) = (\omega^2/\alpha(\omega)^2)$. The terms $-\beta$ in the numerator and $+\beta$ in the denominator of (11a) clearly demonstrate smaller values from this equation compared with the biased ones obtained in conventional

elastography [i.e., with (13)]. It has also been previously shown that including viscoelasticity in the material model decreases the estimated phase velocities and thus the storage modulus [44]. Therefore, the proposed method not only yields the loss modulus in addition to the storage modulus but also improves the estimation of the storage modulus by taking both real and imaginary parts of the wavenumber into account (11a). This is seen in Fig. 5 for the *ex vivo* liver samples, where the assumption of zero dissipation caused a significant overestimation of the storage modulus with the conventional elastography method. The differences were more significant at higher frequencies due to greater values of the imaginary part of the wavenumber (and thus loss modulus) at those frequencies. It also explains higher differences of G' between the proposed method and elastography with castor oil percentages used in the *in vitro* phantoms, i.e., maximum differences of 3% for no oil, 5% for 10% oil, and 10% for 20% oil.

In general, in the case of *ex vivo* liver samples, the postprocessing of experimental data was more straightforward and smoother trends (compared with *in vitro* phantoms) were obtained, especially for the loss modulus. This may be explained by the fact that the decay in shear wave amplitude along the propagation distance [used for the estimation of β in (10a)] is due to two sources: inherent dissipation of the material due to its viscoelasticity [the $e^{-i\beta(\omega)r}$ term in (7)] and the cylindrical geometry of the wave field promoting wave dissipation [the $(1/\sqrt{r})$ term in (7)]. In soft biological samples with an important viscoelasticity component, the inherent dissipation (which is meant to be measured) becomes a more significant source of wave amplitude decay. Therefore, the measurement of the imaginary part of the wavenumber for *ex vivo* liver samples and consequently the loss modulus were less sensitive to the choice of the ROI, experimental noise or other sources of error. This shows the relevance of the proposed method for future *in vivo* viscoelasticity assessment of biological tissues. In contrast, as biological samples are more heterogeneous compared with *in vitro* phantoms, measurements are more sensitive to imaging location. In the case of *ex vivo* liver samples, measurements were thus repeated at different locations and the results were averaged. This is why the coefficient of variation of results was slightly larger for *ex vivo* samples.

An interesting observation in this paper was the greater slopes of shear storage modulus curves versus frequency for samples with higher tan δ, for both *in vitro* and *ex vivo* measurements. This is in good agreement with the fact that highly dissipative viscoelastic materials (high tan δ) show a greater dispersive behavior, i.e., the frequency dependency of the shear wave velocity and thus of the shear storage modulus [36]. It further indicates the reliability of the proposed method and presented results and also suggests that the slope of shear storage modulus curves versus frequency may be regarded as an additional characteristic of viscoelastic materials, as discussed in [45].

One limitation of the proposed method is the assumptions of an isotropic and homogeneous propagation medium, and thus this method may be more relevant for viscoelasticity assessment of macroscopically homogeneous tissues such as the liver. Although most soft biological issues are generally anisotropic and inhomogeneous, especially in the case of glandular and tumorous tissues, conventional ultrasound elastography techniques are nevertheless applied and have been shown to improve the specificity of the diagnosis (e.g., in the case of breast cancer) [9]. The development of a viscoelastography method for reliable model-independent quantification of inhomogeneous media is certainly of future interest but is beyond the scope of this paper.

Another limitation of the proposed method may be the accuracy of the loss modulus estimation for materials with very small dissipation (low viscosity). In this case, the imaginary part of the wavenumber becomes significantly smaller than its real part, and the cylindrical geometry of the wave field may play a more substantial role in shear wave amplitude decay than the inherent viscoelastic properties of the material. This may cause the estimation of the imaginary part of the wavenumber (and thus loss modulus) more sensitive to experimental noise. The proposed method is thus more reliable for complex shear modulus assessment of soft biological tissues, which are usually dissipative [43], [46].

V. Conclusion

A noninvasive ultrasound shear wave viscoelastography method was proposed for model-independent quantification of shear storage and loss moduli as a function of frequency. The proposed method was tested on *in vitro* gelatin-agar phantoms and *ex vivo* porcine liver samples, and the results were found to be in good agreement with those of reference methods. It was shown that the proposed method not only yielded the loss modulus without considering any approximate rheological models but also provided a better estimate of the storage modulus by considering the imaginary part of the shear wavenumber into account. To conclude, the developed viscoelastography method could provide reliable estimates of complex shear modulus over a broad range of frequencies. This method may improve classification of diseases with noninvasive imaging of tissue viscoelasticity.

References

[1] A. P. Sarvazyan, O. V. Rudenko, S. D. Swanson, J. B. Fowlkes, and S. Y. Emelianov, "Shear wave elasticity imaging: A new ultrasonic technology of medical diagnostics," *Ultrasound Med. Biol.*, vol. 24, no. 9, pp. 1419–1435, Dec. 1998.

[2] L. Sandrin *et al.*, "Transient elastography: A new noninvasive method for assessment of hepatic fibrosis," *Ultrasound Med. Biol.*, vol. 29, no. 12, pp. 1705–1713, Dec. 2003.

[3] K. Nightingale, M. S. Soo, R. Nightingale, and G. Trahey, "Acoustic radiation force impulse imaging: *In vivo* demonstration of clinical feasibility," *Ultrasound Med. Biol.*, vol. 28, no. 2, pp. 227–235, Feb. 2002.

[4] J. Bercoff, M. Tanter, and M. Fink, "Supersonic shear imaging: A new technique for soft tissue elasticity mapping," *IEEE Trans. Ultrason., Ferroelectr., Freq. Control*, vol. 51, no. 4, pp. 396–409, Apr. 2004.

[5] G. Montaldo, J. Bercoff, M. Tanter, and M. A. Fink, "Imaging method and apparatus using shear waves," WO Patent 2011132014 A1, Oct. 27, 2011.

[6] N. M. Ivancevich, X. Zeng, and L. Fan, "Swept focus for acoustic radiation force impulse," WO Patent 2015112585 A1, Jul. 30, 2015.

[7] M. Yoneda *et al.*, "Nonalcoholic fatty liver disease: US-based acoustic radiation force impulse elastography," *Radiology*, vol. 256, no. 2, pp. 640–647, 2010.

[8] M. L. Palmeri *et al.*, "Noninvasive evaluation of hepatic fibrosis using acoustic radiation force-based shear stiffness in patients with nonalcoholic fatty liver disease," *J. Hepatol.*, vol. 55, no. 3, pp. 666–672, Sep. 2011.

[9] W. A. Berg *et al.*, "Shear-wave elastography improves the specificity of breast US: The BE1 multinational study of 939 masses," *Radiology*, vol. 262, no. 2, pp. 435–449, 2012.

[10] S. Chen *et al.*, "Assessment of liver viscoelasticity by using shear waves induced by ultrasound radiation force," *Radiology*, vol. 266, no. 3, pp. 964–970, Mar. 2013.

[11] D. Cosgrove *et al.*, "EFSUMB guidelines and recommendations on the clinical use of ultrasound elastography. Part 2: Clinical applications," *Ultraschall Med.*, vol. 34, no. 3, pp. 238–253, 2013.

[12] P. Garteiser *et al.*, "MR elastography of liver tumours: Value of viscoelastic properties for tumour characterisation," *Eur. Radiol.*, vol. 22, no. 10, pp. 2169–2177, Oct. 2012.

[13] M. M. Doyley and K. J. Parker, "Elastography: General principles and clinical applications," *Ultrasound Clin.*, vol. 9, no. 1, pp. 1–11, Jan. 2014.

[14] K.-J. Streitberger *et al.*, "High-resolution mechanical imaging of glioblastoma by multifrequency magnetic resonance elastography," *PLoS ONE*, vol. 9, no. 10, p. e110588, 2014.

[15] Z. S. Xu *et al.*, "Evidence of changes in brain tissue stiffness after ischemic stroke derived from ultrasound-based elastography," *J. Ultrasound Med.*, vol. 32, no. 3, pp. 485–494, Mar. 2013.

[16] D. Chauvet *et al.*, "*In vivo* measurement of brain tumor elasticity using intraoperative shear wave elastography," *Ultraschall Med.*, vol. 36, pp. 1–8, 2015.

[17] H. L. Oestreicher, "Field and impedance of an oscillating sphere in a viscoelastic medium with an application to biophysics," *J. Acoust. Soc. Amer.*, vol. 23, no. 6, pp. 707–714, 1951.

[18] Y. Yamakoshi, J. Sato, and T. Sato, "Ultrasonic imaging of internal vibration of soft tissue under forced vibration," *IEEE Trans. Ultrason., Ferroelectr., Freq. Control*, vol. 37, no. 2, pp. 45–53, Mar. 1990.

[19] S. Chen, M. Fatemi, and J. F. Greenleaf, "Quantifying elasticity and viscosity from measurement of shear wave speed dispersion," *J. Acoust. Soc. Amer.*, vol. 115, no. 6, pp. 2781–2785, 2004.

[20] S. Chen *et al.*, "Shearwave dispersion ultrasound vibrometry (SDUV) for measuring tissue elasticity and viscosity," *IEEE Trans. Ultrason., Ferroelectr., Freq. Control*, vol. 56, no. 1, pp. 55–62, Jan. 2009.

[21] C. Schmitt, A. H. Henni, and G. Cloutier, "Characterization of blood clot viscoelasticity by dynamic ultrasound elastography and modeling of the rheological behavior," *J. Biomech.*, vol. 44, no. 4, pp. 622–629, Feb. 2011.

[22] S. Catheline *et al.*, "Measurement of viscoelastic properties of homogeneous soft solid using transient elastography: An inverse problem approach," *J. Acoust. Soc. Amer.*, vol. 116, no. 6, pp. 3734–3741, 2004.

[23] J. Vappou, C. Maleke, and E. E. Konofagou, "Quantitative viscoelastic parameters measured by harmonic motion imaging," *Phys. Med. Biol.*, vol. 54, no. 11, pp. 3579–3594, 2009.

[24] C. Amador, M. W. Urban, S. Chen, and J. F. Greenleaf, "Loss tangent and complex modulus estimated by acoustic radiation force creep and shear wave dispersion," *Phys. Med. Biol.*, vol. 57, no. 5, pp. 1263–1282, 2012.

[25] S. Kazemirad, H. K. Heris, and L. Mongeau, "Experimental methods for the characterization of the frequency-dependent viscoelastic properties of soft materials," *J. Acoust. Soc. Amer.*, vol. 133, no. 5, pp. 3186–3197, 2013.

[26] S. Kazemirad and L. Mongeau, "Rayleigh wave propagation method for the characterization of viscoelastic properties of biomaterials," *J. Acoust. Soc. Amer.*, vol. 132, no. 3, pp. 4332–4342, 2013.

[27] I. Z. Nenadic *et al.*, "Application of attenuation measuring ultrasound shearwave elastography in 8 post-transplant liver patients," in *Proc. IEEE Int. Ultrason. Symp. (IUS)*, Sep. 2014, pp. 987–990.

[28] N. C. Rouze, M. L. Palmeri, and K. R. Nightingale, "An analytic, Fourier domain description of shear wave propagation in a viscoelastic medium using asymmetric Gaussian sources," *J. Acoust. Soc. Amer.*, vol. 138, no. 2, pp. 1012–1022, 2015.

[29] I. Z. Nenadic *et al.*, "Ultrasound bladder vibrometry method for measuring viscoelasticity of the bladder wall," *Phys. Med. Biol.*, vol. 58, no. 8, p. 2675, 2013.

[30] A. H. Henni, C. Schmitt, and G. Cloutier, "Shear wave induced resonance elastography of soft heterogeneous media," *J. Biomech.*, vol. 43, no. 8, pp. 1488–1493, May 2010.

[31] C. Schmitt, A. H. Henni, and G. Cloutier, "Ultrasound dynamic microelastography applied to the viscoelastic characterization of soft tissues and arterial walls," *Ultrasound Med. Biol.*, vol. 36, no. 9, pp. 1492–1503, Sep. 2010.

[32] E. Montagnon, A. H. Henni, C. Schmitt, and G. Cloutier, "Rheological assessment of a polymeric spherical structure using a three-dimensional shear wave scattering model in dynamic spectroscopy elastography," *IEEE Trans. Ultrason., Ferroelectr., Freq. Control*, vol. 61, no. 2, pp. 277–287, Feb. 2014.

[33] J. Achenbach, *Wave Propagation in Elastic Solids*. Amsterdam, The Netherlands: North Holland, 1973.

[34] K. F. Graff, *Wave Motion in Elastic Solids*. Columbus, OH, USA: Ohio State Univ. Press, 1975.

[35] M. Abramowitz and I. A. Stegun, Eds., *Handbook of Mathematical Functions*. New York, NY, USA: Dover, 1964.

[36] R. Lakes, *Viscoelastic Materials*. New York, NY, USA: Cambridge Univ. Press, 2009.

[37] A. Manduca *et al.*, "Magnetic resonance elastography: Non-invasive mapping of tissue elasticity," *Med. Image Anal.*, vol. 5, no. 4, pp. 237–254, Dec. 2001.

[38] M. Bernal, I. Nenadic, M. W. Urban, and J. F. Greenleaf, "Material property estimation for tubes and arteries using ultrasound radiation force and analysis of propagating modes," *J. Acoust. Soc. Amer.*, vol. 129, no. 3, pp. 1344–1354, 2011.

[39] L. Allard, G. Soulez, B. Chayer, Z. Qin, D. Roy, and G. Cloutier, "A multimodality vascular imaging phantom of an abdominal aortic aneurysm with a visible thrombus," *Med. Phys.*, vol. 40, no. 6, pp. 063701-1–063701-10, 2013.

[40] A. Ouared, E. Montagnon, S. Kazemirad, L. Gaboury, A. Robidoux, and G. Cloutier, "Frequency adaptation for enhanced radiation force amplitude in dynamic elastography," *IEEE Trans. Ultrason., Ferroelectr., Freq. Control*, vol. 62, no. 8, pp. 1453–1466, Aug. 2015.

[41] E. Montagnon, S. Hissoiny, P. Després, and G. Cloutier, "Real-time processing in dynamic ultrasound elastography: A GPU-based implementation using CUDA," in *Proc. 11th Int. Conf. Inf. Sci., Signal Process. Appl. (ISSPA)*, Jul. 2012, pp. 472–477.

[42] J.-L. Gennisson, A. Marcellan, A. Dizeux, and M. Tanter, "Rheology over five orders of magnitude in model hydrogels: Agreement between strain-controlled rheometry, transient elastography, and supersonic shear wave imaging," *IEEE Trans. Ultrason., Ferroelectr., Freq. Control*, vol. 61, no. 6, pp. 946–954, Jun. 2014.

[43] D. Klatt, C. Friedrich, Y. Korth, R. Vogt, J. Braun, and I. Sack, "Viscoelastic properties of liver measured by oscillatory rheometry and multifrequency magnetic resonance elastography," *Biorheology*, vol. 47, no. 2, pp. 133–141, 2010.

[44] A. Caenen *et al.*, "A versatile and experimentally validated finite element model to assess the accuracy of shear wave elastography in a bounded viscoelastic medium," *IEEE Trans. Ultrason., Ferroelectr., Freq. Control*, vol. 62, no. 3, pp. 439–450, Mar. 2015.

[45] K. J. Parker, A. Partin, and D. J. Rubens, "What do we know about shear wave dispersion in normal and steatotic livers?" *Ultrasound Med. Biol.*, vol. 41, no. 5, pp. 1481–1487, May 2015.

[46] R. Sinkus, M. Tanter, T. Xydeas, S. Catheline, J. Bercoff, and M. Fink, "Viscoelastic shear properties of *in vivo* breast lesions measured by MR elastography," *Magn. Reson. Imag.*, vol. 23, no. 2, pp. 159–165, Feb. 2005.

Siavash Kazemirad received the B.Sc. degree in mechanical engineering from the Iran University of Science and Technology, Tehran, Iran, in 2006, the M.Sc. degree in mechanical engineering from the Sharif University of Technology, Tehran, in 2009, with a minor in biomechanics, and the Ph.D. degree in mechanical engineering from McGill University, Montréal, QC, Canada, in 2013.

He was with the Biomechanics Research Laboratory, McGill University. Upon completing his Ph.D. study in 2013, he joined the Laboratory of Biorheology and Medical Ultrasonics, University of Montreal Hospital Research Centre, Montréal, as a Postdoctoral Fellow. His current research interests include vibration and acoustics, wave propagation, ultrasound imaging, material characterization, and ultrasound elastography.

Simon Bernard was born in Quimper, France, in 1988. He received the master's degree and the Ph.D. degree in physical acoustics from Université Pierre et Marie Curie, Paris, France, in 2011 and 2014, respectively. His Ph.D. work focused on the measurement of bone mechanical properties using ultrasound methods.

He is currently a Postdoctoral Fellow with the Laboratory of Biorheology and Medical Ultrasonics, University of Montreal Hospital Research Center, Montréal, QC, Canada, where he is involved in the field of shear wave elastography. His current research interests include ultrasound methods for material characterization, modeling of wave propagation and scattering, and inverse problem solutions.

Samuel Hybois received the B.Sc. degree in materials engineering from the École Nationale Supérieure des Mines de Nancy, Nancy, France, in 2014. He is currently pursuing the M.Sc. degree in biomechanics with Arts et Métiers ParisTech, Paris, France, with a specialization in musculoskeletal modeling applied to sports, disability, and rehabilitation.

He joined the Laboratory of Biorheology and Medical Ultrasonics, University of Montreal Hospital Research Center, Montréal, QC, Canada, in 2015, as a Research Intern, supported by the Mitacs Globalink Scholarship.

An Tang was born in Ho Chi Minh City, Vietnam, in 1977. He received the M.D. degree from the University of Sherbrooke, Sherbrooke, QC, Canada, in 2000, and the M.Sc. degree in biomedical sciences from the Université de Montréal, Montréal, QC, Canada, in 2012.

He completed his Radiology residency with the Université de Montréal in 2005. He pursued fellowship training in abdominal imaging with the University of Toronto, Toronto, ON, Canada, in 2006. From 2006 to 2011, he practiced as an Abdominal Radiologist with the Centre Hospitalier de l'Université de Montréal, Montréal. Supported by fellowship awards from the Fulbright Program and the Canadian Institutes of Health Research, he pursued a research fellowship in liver elastography with the University of California at San Diego, San Diego, CA, USA, from 2011 to 2012. He is currently a Clinical Researcher with the Centre de Recherche du Centre Hospitalier de l'Université de Montréal and an Associate Professor of Radiology with the Université de Montréal. His current research interests include imaging-based techniques for diagnosis and monitoring of chronic liver disease, including biomarkers of liver fat, inflammation, and fibrosis.

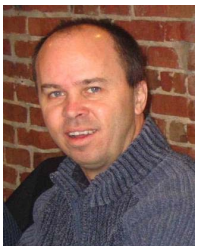

Guy Cloutier (S'89–M'90–SM'07) received the B.Eng. degree in electrical engineering from the Université du Québec à Trois-Rivières, Trois-Rivières, QC, Canada, and the M.Sc. and Ph.D. degrees in biomedical engineering from the École Polytechnique of Montréal, Montréal, QC, Canada, in 1984, 1986, and 1990, respectively.

He was a Postdoctoral Fellow with The Pennsylvania State University, State College, PA, USA, with Prof. K. K. Shung from 1990 to 1992. He is currently the Director of the Laboratory of Biorheology and Medical Ultrasonics with the University of Montreal Hospital Research Center, Montréal, where he is a Professor with the Department of Radiology, Radio-Oncology, and Nuclear Medicine, and a member of the Institute of Biomedical Engineering with the Université de Montréal, Montréal. He has authored over 175 peer-reviewed articles in his research fields, holds 12 patents, and licensed two technologies. His current research interests include quantitative ultrasound imaging of red blood cell aggregation, liver, tendon, and vascular diseases; quasi-static and dynamic ultrasound elastography of atherosclerotic plaques, vascular aneurysms, deep vein thrombi, breast cancers, and liver steatosis; development of multiphysics imaging methods; and mathematical and biomechanical modeling.

Dr. Cloutier was a recipient of the National Scientist Award of the Fonds de la Recherche en Santé du Québec from 2004 to 2009. He is an Associate Editor of the IEEE TRANSACTIONS ON ULTRASONICS, FERROELECTRIC AND FREQUENCY CONTROL, an Invited Associate Editor of *Medical Physics*, and a member of the Editorial Board of *Current Medical Imaging Reviews*, and was a member of the International Advisory Editorial Board of *Ultrasound in Medicine and Biology* for 15 years.